Methodology and Computing in Applied Probability
https://doi.org/10.1007/s11009-019-09738-0

Stochastic Reconstruction for Inhomogeneous Point Patterns

Kateřina Koňasová[1] · **Jiří Dvořák**[1]

Received: 3 January 2019 / Revised: 26 July 2019 / Accepted: 31 July 2019 /
Published online: 15 August 2019
© Springer Science+Business Media, LLC, part of Springer Nature 2019

Abstract

The stochastic reconstruction approach for point processes aims at producing independent patterns with the same properties as the observed pattern, without specifying any particular model. Instead a so-called energy functional is defined, based on a set of point process summary characteristics. It measures the dissimilarity between the observed pattern (input) and another pattern. The reconstructed pattern (output) is sought iteratively by minimising the energy functional. Hence, the output has approximately the same values of the prescribed summary characteristics as the input pattern. In this paper, we focus on inhomogeneous point patterns and apply formal hypotheses tests to check the quality of reconstructions in terms of the intensity function and morphological properties of the underlying point patterns. We argue that the current version of the algorithm available in the literature for inhomogeneous point processes does not produce outputs with appropriate intensity function. We propose modifications to the algorithm which can remedy this issue.

Keywords Stochastic reconstruction · Point process · Summary characteristics · Inhomogeneous process · Intensity function

Mathematics Subject Classification (2010) 60G55

We are grateful to the reviewers for their insightful comments and suggestions. We are also grateful to Thorsten Wiegand for the discussion and helpful comments about stochastic reconstruction and to Rasmus P. Waagepetersen for drawing our attention to the simulated tempering approach. This work has been supported by The Charles University Grant Agency, project no. 472217, and The Czech Science Foundation, project no. 19-04412S.

Electronic supplementary material The online version of this article (https://doi.org/10.1007/s11009-019-09738-0) contains supplementary material, which is available to authorized users.

✉ Jiří Dvořák
dvorak@karlin.mff.cuni.cz

[1] Department of Probability and Mathematical Statistics, Faculty of Mathematics and Physics, Charles University, Sokolovská 83, 186 75, Praha 8, Czech Republic

1 Introduction

Simulations are often used in spatial statistics for Monte Carlo testing and studying the performance of different inferential procedures. A fully specified model is required to perform the simulations, e.g. a benchmark model such as the Complete Spatial Randomness model for spatial point processes or perhaps a model fitted to the observed data. However, sometimes a particular model may not be available or the principal interest may lie in producing independent realisations with the same properties as the observed data rather than in fitting a parametric model. In such a case it is possible to use the so-called stochastic reconstruction approach to produce such realisations. It has been used for nearly two decades in statistical physics to generate random closed sets, typically as models for porous media, see Torquato (2002).

In this paper we focus on the stochastic reconstruction for point processes, also called pattern reconstruction in this setting. For stationary point processes, it has been proposed in Tscheschel and Stoyan (2006) and in a slightly different version in Pommerening (2006). The paper Tscheschel and Stoyan (2006) also suggests the so-called conditional reconstruction which enables to extend the observed point pattern outside the boundaries of the observation window, conditionally on the observed point pattern, see also Illian et al. (2004). This has been used in the literature as a form of quasi-plus-sampling for mitigating the edge-effects, see e.g. Lilleleht et al. (2014) or Tscheschel and Chiu (2008). Stochastic reconstruction has found another application in ecological works in Monte Carlo testing of independence in a bivariate point process, see e.g. Getzin et al. (2014) and Jacquemyn et al. (2012) or Mundo et al. (2013). On similar grounds, a non-parametric test of isotropy of a stationary point process based on stochastic reconstruction is proposed in Wong and Chiu (2016).

The stochastic reconstruction algorithm aims at producing a pattern (output) with the same properties as the observed pattern (input). The user needs to choose which properties are to be maintained by the algorithm, by selecting a collection of summary characteristics $f_1, \ldots, f_J$ such as the pair-correlation function, spherical contact distribution function, etc. These characteristics are then used to construct the so-called energy functional which measures the dissimilarity between the input and another point pattern in terms of discrepancies between the summary characteristics estimated from the two patterns. Then the energy functional is iteratively minimised so that the summary characteristics of the output pattern match those of the input as closely as possible. The ultimate goal is that the reconstructions have the same distribution as the input, i.e. any possible summary characteristic of the output is close to that of the input.

An interesting application of stochastic reconstruction can be found in Wiegand et al. (2013) where the authors investigate which summary characteristic carries the most information about given datasets. This enables them to make suggestions which characteristics should be used in ecological studies to describe the point patterns under study. Their approach is based on reconstructing the patterns using a small set of summary characteristics and studying how well other characteristics of the outputs match those of the input.

Also, the paper Wiegand et al. (2013) discusses, to the best of our knowledge, for the first time how to perform stochastic reconstruction for inhomogeneous point processes, i.e. for processes with non-constant intensity function. Working with inhomogeneous point patterns brings in difficult problems such as, for clustered patterns, the relationship between clustering and inhomogeneity. This cannot be disentangled based on the observed pattern only, without expert knowledge of the problem at hand. The user has to decide whether

local changes in the intensity of point occurrence result from clustering or inhomogeneity and adapt the inference accordingly.

For visual check of the quality of reconstructions the paper Wiegand et al. (2013) uses envelopes for summary characteristics constructed from several outputs. However, a formal test was not considered there. We elaborate on this by applying a rank envelope test (Mrkvička et al. 2018; Myllymäki et al. 2017) which can provide a p-value as well as a graphical interpretation indicating the reason for possible rejection.

Furthermore, we focus on inhomogeneous point processes and propose a formal hypothesis test to investigate if the intensity function of outputs matches correctly the intensity function of the input. Based on previous experiments in Koňasová (2018) we believe that the version of the algorithm proposed in Wiegand et al. (2013) is often not successful in reconstructing the intensity function. Therefore we propose modifications to the algorithm that can remedy this issue. We illustrate this in the current paper by means of simulation experiments.

Although we consider several different energy functionals in our simulations, it is not our intention here to identify a single best energy functional and optimal version of the algorithm (if such things exist at all, since different patterns may require different approaches). Instead, we believe that a user of stochastic reconstruction should first perform a simulation study with a model producing point patterns similar to the pattern of interest and use the tests described here to identify which summary characteristics to incorporate to the energy functional, with which weights, which stopping rule to use, etc.

We remark that in this paper we consider the *improvement only* version of the iterative optimisation procedure which makes it impossible to leave a local minimum of the energy functional. This version is the one most frequently appearing in the literature. However, several authors have remarked that a version using the Metropolis-Hastings algorithm can be used instead. Our experience indicates that properly tuning up such an algorithm is a challenging task and the outcome is most likely not worth the effort, despite good theoretical properties of the Markov chain, see Koňasová (2018, Chapter 4). In fact we believe that good mixing properties of the Markov chain, i.e. the ability to explore well the whole space of point configurations, prevents the chain from regularly visiting states with very low energy. The simulated tempering method seems to provide a reasonable alternative.

The paper is organised as follows. In Section 2 the necessary theory about spatial point processes and their summary characteristics is reviewed. Section 3 introduces the stochastic reconstruction algorithm and its possible modifications for inhomogeneous point processes. In Section 4 a methodology for assessing the quality of reconstruction is discussed and formal tests are proposed. The performance of the stochastic reconstruction algorithm is studied in the simulation experiments in Section 5. We conclude with a discussion in Section 6.

2 Background on Spatial Point Processes

In this section, we introduce the notation and recall basic definitions regarding spatial point processes and their summary characteristics. For more detailed exposition about point processes see e.g. Daley and Vere-Jones (2008), Illian et al. (2004), and Møller and Waagepetersen (2004).

We consider a simple spatial point process X to be a random locally finite subset of $\mathbb{R}^2$. The points $x \in X$ correspond to certain objects or events occurring at $x \in \mathbb{R}^2$. The Borel σ-algebra on $\mathbb{R}^2$ is denoted by $\mathfrak{B}^2$. The area of $B \in \mathfrak{B}^2$ is denoted by $|B|$ and $\mathbf{1}$ is the indicator function.

2.1 Moment Properties and Summary Characteristics of Point Processes

The intensity measure Λ of the point process X is given by the formula

$$\Lambda(B) = \mathbb{E}[N_X(B)], \quad B \in \mathfrak{B}^2,$$

where $N_X(B)$ is the (random) number of points of the process X in the set B. Similarly, we denote by $N(A)$ the (non-random) number of elements in a deterministic finite set A. If Λ is absolutely continuous with respect to the two-dimensional Lebesgue measure, there exists a non-negative measurable function λ such that

$$\Lambda(B) = \int_B \lambda(u)\,\mathrm{d}u \quad \forall\, B \in \mathfrak{B}^2.$$

The function λ is called the intensity function of X.

The process X is said to be homogeneous if its intensity measure Λ is translation invariant. Otherwise, X is said to be inhomogeneous. Moreover, X is stationary if the whole distribution of X is translation invariant. Note that stationarity of X implies its homogeneity but not vice versa. For a homogeneous point process, the intensity function λ exists and is constant. This constant is called the intensity of X.

The second-order factorial moment measure $\alpha^{(2)}$ is given by

$$\alpha^{(2)}(C) = \mathbb{E}\sum_{x,y\in X}^{\neq} \mathbf{1}\{(x,y) \in C\}, \quad C \in \mathfrak{B}^2 \otimes \mathfrak{B}^2.$$

The symbol $\neq$ indicates that the summation is over pairs of distinct points. If $\alpha^{(2)}$ is absolutely continuous with respect to the four-dimensional Lebesgue measure, there exists a non-negative measurable function $\lambda^{(2)}$ such that

$$\alpha^{(2)}(C) = \int_{\mathbb{R}^2}\int_{\mathbb{R}^2} \mathbf{1}\{(u,v) \in C\}\ \lambda^{(2)}(u,v)\,\mathrm{d}u\,\mathrm{d}v, \quad C \in \mathfrak{B}^2 \otimes \mathfrak{B}^2.$$

The function $\lambda^{(2)}$ is called the second-order product density of X.

Assuming that λ and $\lambda^{(2)}$ exist we define the pair correlation function g as

$$g(u,v) = \frac{\lambda^{(2)}(u,v)}{\lambda(u)\lambda(v)}, \quad \text{for } u, v \in \mathbb{R}^2 \text{ such that } \lambda(u), \lambda(v) > 0.$$

If $\lambda(u) = 0$ or $\lambda(v) = 0$ we set $g(u,v) = 0$. If the pair correlation function $g(u,v)$ is translation invariant we write with slight abuse of notation $g(u,v) = g(u-v)$ and we define the K- and L-functions as

$$K(r) = \int_{b(o,r)} g(z)\,\mathrm{d}z, \quad r > 0, \qquad L(r) = \sqrt{\frac{K(r)}{\pi}}, \quad r > 0,$$

where $b(o,r)$ denotes the ball centred at the origin o with radius r. The assumption $g(u,v) = g(u-v)$ is fulfilled for stationary point processes or the second-order intensity reweighted stationary (SOIRS) point processes (Baddeley et al. 2000). Note that the K-function can be also defined in a more general way, see e.g. Illian et al. (2004).

The functions g, K and L introduced above are second-order summary characteristics and contain information about the interactions between pairs of points. For a Poisson process in $\mathbb{R}^2$ with a (constant or non-constant) intensity function we have that $g(u) \equiv 1$, $K(r) = \pi r^2$ and $L(r) = r$, $r > 0$. These values serve as a benchmark of no interactions between pairs of points.

The nearest-neighbour distance distribution function D_1, which is a characteristic based on interpoint distances, is defined for a stationary point process as

$$D_1(r) = \frac{1}{\lambda|A|}\,\mathbb{E}\sum_{x\in X\cap A}\mathbf{1}\left\{N_{X\setminus\{x\}}\left(b(x,r)\right)>0\right\},\quad r>0,$$

where $A \in \mathfrak{B}^2$ is an arbitrary set satisfying $0 < |A| < \infty$. Stationarity implies that the definition does not depend on the choice of A. D_1 can be interpreted as the distribution function of the distance from a typical point of the process X to its nearest neighbour (see Appendix C of Møller and Waagepetersen (2004) for further details). We remark that the nearest neighbour distance distribution function is often denoted G but we follow here the notation from the paper (Tscheschel and Stoyan 2006). Similarly, the k-th nearest neighbour distance distribution functions $D_k, k = 2, 3, \ldots,$ can be defined for stationary point processes, see Stoyan and Stoyan (1994, p.267).

The spherical contact distribution function F of a stationary point process X is the distribution function of the distance from the origin (or, due to stationarity, any fixed point in $\mathbb{R}^2$) to the nearest point of the process. It carries information about the size of gaps between the points of the process and is formally defined as

$$F(r) = \mathbb{P}\left[N_X\left(b(o,r)\right)>0\right],\quad r>0.$$

2.2 Non-Parametric Estimation

Assume now that the point process X is observed on a compact observation window $W \subset \mathbb{R}^2$ such that $0 < |W| < \infty$. In the following, we recall the non-parametric estimators of the summary characteristics discussed above.

If X has a constant intensity function λ a natural estimator of λ is $\widehat{\lambda} = N_X(W)/|W|$. If X has a non-constant intensity function $\widehat{\lambda}$ can be obtained using a kernel estimator. Let k be a probability density function on $\mathbb{R}^2$ and define the kernel with bandwidth $b > 0$ as $k_b(x) = k(\frac{x}{b})/b^2$. The estimator of λ is given by

$$\widehat{\lambda(x)} = \frac{1}{C_{W,b}(x)}\sum_{y\in X\cap W}k_b(x-y),\quad x\in W, \tag{1}$$

where $C_{W,b}(x) = \int_W k_b(x-y)\,\mathrm{d}y$ is the edge-correction factor.

The classical estimator of the pair correlation function g, assuming its translation invariance, is given by

$$\widehat{g}(r) = \sum_{x,y\in X\cap W}^{\neq}\frac{u_b\left(r-\|x-y\|\right)}{2\pi r\widehat{\lambda(x)}\widehat{\lambda(y)}}\frac{1}{|W\cap(W+x-y)|},\quad r>0,$$

where u_b is a one-dimensional kernel function with bandwidth $b > 0$ and we employ the translation edge-correction. For other edge-correction methods see Illian et al. (2004, Section 4.2.2). The estimator of the K-function, again using the translation edge correction, has the form

$$\widehat{K}(r) = \sum_{x,y\in X\cap W}^{\neq}\frac{\mathbf{1}\{\|x-y\|\le r\}}{\widehat{\lambda(x)}\widehat{\lambda(y)}|W\cap(W+x-y)|},\quad r>0.$$

The estimator of $L(r)$ is obtained by $\widehat{L}(r) = \sqrt{\frac{\widehat{K}(r)}{\pi}}, r > 0$.

Under stationarity of X, the raw estimator of the k-th nearest-neighbour distance distribution function $D_k, k = 1, 2, \ldots$, is given by

$$\widehat{D}_k(r) = \frac{1}{N_X(W)} \sum_{x \in X \cap W} \mathbf{1}\{e_k(x) \leq r\}, \quad r > 0, \tag{2}$$

where $e_k(x)$ is the distance of the point $x \in X$ to its k-th nearest neighbour in $X \cap W$.

For estimation of the spherical contact distribution function F, under the stationarity assumption, consider a regular grid I_a of points in $\mathbb{R}^2$,

$$I_a = y + a\mathbb{Z}^2 = \left\{(y_1 + a_1 z_1, y_2 + a_2 z_2) \in \mathbb{R}^2 : z_i \in \mathbb{Z}\right\}, \quad r > 0,$$

where $y = (y_1, y_2) \in \mathbb{R}^2$ and $a = (a_1, a_2) \in \mathbb{R}^2$ such that $a_1, a_2 > 0$. The estimator of F is given by

$$\widehat{F}(r) = \frac{1}{N(I_a \cap W)} \sum_{x \in I_a \cap W} \mathbf{1}\{d(x, X \cap W) \leq r\}, \quad r > 0, \tag{3}$$

where $d(x, X \cap W)$ denotes the distance from x to the nearest point of the process X lying in W. This is again the so-called raw estimator with no edge-correction. For edge-correction methods such as the reduced-sample approach or the Kaplan-Meier estimator see e.g. Møller and Waagepetersen (2004, Section 4.3.6).

2.3 Morphological Characteristics of Point Patterns

For checking the quality of reconstructions we use in this paper the three Mecke's morphological characteristics of point patterns (Mecke and Stoyan 2005) defined in the following way. Let ζ be a point pattern in the observation window W and let $Z(r) = (\zeta \oplus b(o, r)) \cap W, r > 0$, where $b(o, r)$ is the ball of radius r centred at the origin, i.e. $Z(r)$ is the union of discs with radius r centred at the points of ζ, intersected with W. Denote $A(r)$, $L(r)$ and $\chi(r)$ the area, boundary length and the Euler-Poincaré characteristic of $Z(r)$, respectively, as functions of the radius r.

3 Stochastic Reconstruction

Stochastic reconstruction is an algorithmic procedure that aims at producing point patterns with similar properties as the observed point pattern. To achieve this we define a dissimilarity measure, called the *energy functional* in the following, and apply an iterative optimisation scheme for its minimisation. The choice of summary characteristics to be incorporated into the energy functional determines which properties of the observed pattern (*input*) are required to be similar in the reconstructed patterns (*outputs*).

From now on we assume that we observe a realisation $\mathcal{X}$ of a point process X on a compact observation window $W \subset \mathbb{R}^2$ such that $0 < |W|$. We also assume that the intensity function λ and the second-order product density $\lambda^{(2)}$ of X exist.

We first describe in Section 3.1 the stochastic reconstruction algorithm for stationary point processes as given in Tscheschel and Stoyan (2006) and Illian et al. (2004) and briefly mention the conditional reconstruction in Section 3.2. Then we discuss in Section 3.3 a version for inhomogeneous point processes given in Wiegand et al. (2013) and we propose some further modifications in Section 3.4.

3.1 The Algorithm

In this section, we assume $\mathcal{X}$ is a realisation of a stationary point process X. Take $J \in \mathbb{N}$ and choose functional summary characteristics f_j, $j = 1, 2, \ldots, J$, such as those described in Section 2.1. Numerical characteristics can be also incorporated in a natural way. For every functional characteristic f_j choose an upper bound R_j for its domain, possibly depending on the size of the observation window W and the assumed scale of effects to be investigated. By $\widehat{f_j}(\mathcal{X}, r)$ we denote the empirical estimate of $f_j(r)$ computed from $\mathcal{X}$. We remark that the use of the stochastic reconstruction does not require any explicit assumptions on the theoretical model for observed data since in fact only the empirical estimates $\widehat{f_j}(\mathcal{X}, r)$ will be used.

The algorithm aims at creating an artificial pattern ζ in W such that

$$\widehat{f_j}(\zeta, r) \approx \widehat{f_j}(\mathcal{X}, r),\ 0 < r \le R_j,\ j = 1, 2, \ldots, J.$$

Also, the algorithm is designed such that the number of points in the point patterns is fixed, $N(\zeta \cap W) = N(\mathcal{X} \cap W)$. The dissimilarity between $\mathcal{X}$ and ζ is measured by the energy functional E which is given by the weighted sum

$$E(\mathcal{X}, \zeta) = \sum_{j=1}^{J} w_{f_j} \int_0^{R_j} \left[\widehat{f_j}(\mathcal{X}, r) - \widehat{f_j}(\zeta, r)\right]^2 \mathrm{d}r, \tag{4}$$

where $w_{f_j} > 0$, $j = 1, 2, \ldots, J$, are the weights determining the relative importance of the individual terms. Note that the weights should also reflect the possibly different scales of the values of different summary characteristics. The weights can be chosen experimentally, after several trial runs of the algorithm, or based on the expert knowledge of the data. We remark that using only empirical distribution functions in the energy functional makes the choice of weights very straightforward. Instead of scalar weights one might consider weight functions and use the terms

$$\int_0^{R_j} w_{f_j}(r) \left[\widehat{f_j}(\mathcal{X}, r) - \widehat{f_j}(\zeta, r)\right]^2 \mathrm{d}r$$

to construct the energy functional. This choice can be beneficial e.g. to compensate for the possibly non-constant variance of $\widehat{f_j}(\cdot, r)$.

Example 1 Suppose that we have observed a point pattern $\mathcal{X}$ in the observation window $W = [0, 1]^2$ and that, based on the prior knowledge of the problem at hand, the pair correlation function g describes the properties of $\mathcal{X}$ that are of the main interest. Thus $J = 1$,

$f_1 = g$, $w_g = 1$ and $R_1 = 0.25$ (based on the standard recommendations related to the size of W). Then, for a point configuration ζ in W, we have

$$E(\mathcal{X}, \zeta) = \int_0^{0.25} \left[\widehat{g}(\mathcal{X}, r) - \widehat{g}(\zeta, r)\right]^2 \, \mathrm{d}r.$$

Denote by $n = N(\mathcal{X} \cap W)$ the number of observed points. The (random) initial state $\zeta^{(0)}$ of the stochastic reconstruction algorithm is a configuration of n points in W placed independently with uniform distribution in W. The sequence of configurations $\zeta^{(1)}, \zeta^{(2)}, \ldots$, is obtained iteratively as follows. Suppose the current state is $\zeta^{(l)}$, then

- choose randomly, with probabilities $\frac{1}{n}$, a point z from the configuration $\zeta^{(l)}$ to be deleted,
- generate a new point y uniformly in W,
- set $\zeta^{new} = \left(\zeta^{(l)} \setminus \{z\}\right) \cup \{y\}$,
- if $E\left(\mathcal{X}, \zeta^{new}\right) \leq E\left(\mathcal{X}, \zeta^{(l)}\right)$, set $\zeta^{(l+1)} = \zeta^{new}$; otherwise $\zeta^{(l+1)} = \zeta^{(l)}$.

The proposals for deleting and adding points are independent of each other and also independent of the proposals made in other iteration steps. The algorithm is stopped when a given stopping criterion is met, e.g. a specified maximum number of iterations is reached, or $E\left(\mathcal{X}, \zeta^{(l)}\right) < \varepsilon$ for some fixed $\varepsilon > 0$, or the proposed configuration ζ^{new} was not accepted for $m \in \mathbb{N}$ consecutive steps.

The proposals for deleting a point and adding a new one can be of course interpreted as a proposal to move a single point. Clearly, the number of points does not change during an iteration step. The stopping rule should be specified so that every point of the initial configuration has a chance to be moved several times.

Example 1 (continued) Suppose we observed a clustered point pattern given in Fig. 1 (left). We define the energy functional based on the pair-correlation function only as in the Example 1 above. The algorithm is stopped if a new configuration has not been accepted for 100 times in a row. Three different outputs from three independent runs of the stochastic reconstruction algorithm (stationary version) are given in Fig. 1. Evolution of the values of the energy functional during these three runs of the algorithm is depicted in Figure S1 in Online Resource 1.

The core of the algorithm above is the minimisation of the energy functional $E(\mathcal{X}, \zeta)$ w.r.t. ζ while keeping the input $\mathcal{X}$ fixed. During the run of the algorithm, a local minimum

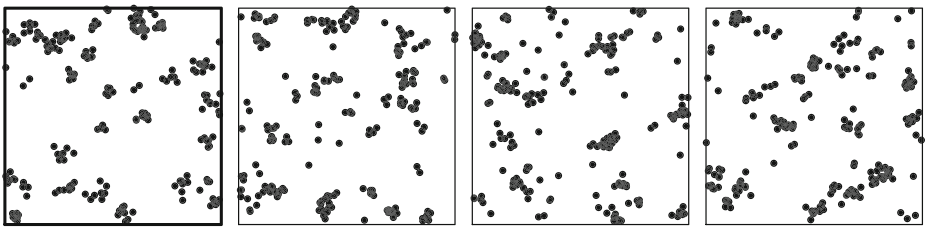

Fig. 1 Illustration of the stochastic reconstruction approach in the stationary context. From left to right: input of the algorithm, three different outputs from three different runs of the algorithm. The energy functional is based on the pair correlation function g only, see Example 1

of $E(\mathcal{X}, \cdot)$ is reached. With the *improvement-only* type of algorithm given above it is not possible to leave a local minimum since no configurations with higher energy are accepted. This can be remedied by running $k \in \mathbb{N}$ independent runs of the algorithm with the same input but different initial configurations, producing k candidate outputs corresponding to different local minima and selecting the candidate with the lowest energy.

Of course $E(\mathcal{X}, \mathcal{X}) = 0$ and hence at least one global minimum of the energy functional exists. However, the aim is not to obtain a copy of the observed data but a different pattern with the same properties and the outputs from local minima with very low energy are satisfactory for this purpose.

3.2 Conditional Reconstruction

The algorithm given above can be easily extended to the situation where the pattern $\mathcal{X}$ is observed in the window W but the reconstructed pattern ζ is required in a bigger window $\widetilde{W} \supset W$ while keeping $\mathcal{X} \subset \zeta$ (Tscheschel and Stoyan 2006; Illian et al. 2004). We use the term *conditional reconstruction* for this modification as in Illian et al. (2004) while in Tscheschel and Stoyan (2006) it is called *conditional simulation*. We prefer the former term since the procedure is in spirit closer to the reconstruction (producing independent replicates with the same properties) than to simulation from a specific model.

Assuming that $\mathcal{X}$ is a realisation of a stationary process X observed in W, we estimate the intensity of X as $\widehat{\lambda} = N(\mathcal{X} \cap W)/|W|$. The number of points for the configuration ζ we seek is then chosen to be $m = \lfloor \widehat{\lambda} |\widetilde{W}| \rfloor$ and it will be fixed during the iterative procedure. Let $n = N(\mathcal{X} \cap W)$ and take ξ a configuration of $m - n$ independent points distributed uniformly in $\widetilde{W} \setminus W$. Then $\zeta^{(0)} = \xi \cup \mathcal{X}$ will be the initial configuration for the reconstruction algorithm. In the iteration steps only the points in $\zeta^{(l)} \setminus \mathcal{X}$ can be deleted with equal probabilities and new points are proposed only in $\widetilde{W} \setminus W$.

The energy functional given by (4) can be used also in this context. However, we stress that the configurations $\mathcal{X}$ and $\zeta^{(l)}$ have a different number of points and correspond to different observation windows. Hence only edge-corrected empirical estimates of the summary characteristics must be used so that comparing $\widehat{f}_j(\mathcal{X}, \cdot)$ to $\widehat{f}_j(\zeta^{(l)}, \cdot)$ makes sense.

3.3 Stochastic Reconstruction for Inhomogeneous Point Patterns

We now discuss the extension of the stochastic reconstruction algorithm to the processes with non-constant intensity function. We describe first the version proposed in Wiegand et al. (2013). Suppose that $\mathcal{X}$ is a realisation of a SOIRS process X observed in W for which the functions λ, $\lambda^{(2)}$ and g exist and that λ is not constant.

Let $\widehat{\lambda}_{\mathcal{X}}$ be the non-parametric estimate of the intensity function based on $\mathcal{X}$, as given in (1). Also, let the observed number of points be denoted by n. The stochastic reconstruction algorithm is the same as given in Section 3.1 with only two changes:

- the initial configuration $\zeta^{(0)}$ of the stochastic reconstruction algorithm is now a configuration of n independent points in W distributed according to the probability density function proportional to $\widehat{\lambda}_{\mathcal{X}}$ restricted to W,
- the proposals for new points are not made uniformly in W but according to the probability density function proportional to $\widehat{\lambda}_{\mathcal{X}}$ as above.

3.4 Proposed Modification

In the simulation experiments in Section 5 we will show that the two modifications discussed above are not sufficient to produce satisfactory outputs – the intensity function is not matched correctly. This is not surprising since the inhomogeneity is incorporated into the algorithm only in the proposals. Hence we propose below a further improvement to the algorithm. The modification consists of adding an extra term to the energy functional which enforces the correct shape of the intensity function.

Consider a regular pixel grid $\{v_1, \ldots, v_I\} \subset W$ with pixel area a and a finite point configuration $\zeta \subset W$. Let

$$\Delta(\mathcal{X}, \zeta) = \sum_{i=1}^{I} a \left[\widehat{\lambda}_{\mathcal{X}}(v_i) - \widehat{\lambda}_{\zeta}(v_i)\right]^2$$

be the Riemann approximation to the integral of the squared difference between the estimated intensity functions computed from the input $\mathcal{X}$ and the configuration ζ. The term $\Delta(\mathcal{X}, \zeta)$ can be added to the energy functional (4) with weight w_Δ. It contains information about the whole surface of the intensity function, thus enforcing the same values of intensity function to appear at the same places in both the input and the outputs. Example of the run of the algorithm based on energy functional incorporating Δ is given in Online Resource 1, see Figure S2.

In certain situations it may be appropriate to allow some changes in the intensity function to occur during the reconstruction process – e.g. in clustered point patterns, it may be relevant to let the clusters appear at different locations in the outputs than in the input. In such a case the term $\Delta(\mathcal{X}, \zeta)$ in (4) can be replaced by the empirical distribution function Γ of the values of the estimated intensity function $\widehat{\lambda}$ sampled in the pixel grid $\{v_1, \ldots, v_I\} \subset W$. With this modification, the correct values of the intensity function are forced to appear in the outputs in correct proportions in places possibly different from the input. Note that in this context we somewhat abuse the term *intensity* function and in fact mean, in case of clustered point processes assumed to be Cox processes, the realisation of the random driving field rather than its expectation.

4 Checking the Quality of Reconstruction

In Wiegand et al. (2013) envelopes for summary characteristics constructed from several outputs were used for visual assessment of the quality of reconstruction. We elaborate on this by proposing a formal hypothesis test using the Monte Carlo approach and either scalar or functional test statistics. We distinguish two cases: either the model generating the observed pattern is not known (as common in practice) or it is known (as in simulation studies). For the latter case, we also propose a test for checking if the intensity function of the inputs is matched correctly in the outputs.

4.1 Testing in Practice

The typical situation in applications is that the process X generating the observed pattern $\mathcal{X}$ is not known. Assume that a set of N outputs $\zeta_1, \ldots, \zeta_N$ based on the input $\mathcal{X}$ has been produced. Heuristically speaking, the reconstruction procedure can be considered satisfactory if the pattern $\mathcal{X}$ is typical among $\zeta_1, \ldots, \zeta_N$.

Formally, let Z be a random output of the stochastic reconstruction based on a random input (having the distribution which generated $\mathcal{X}$) and let T be a test statistic. The distribution of $T(Z)$ can be approximated by $T(\zeta_1), \ldots, T(\zeta_N)$. We aim at testing if $T(\mathcal{X})$ can be considered a realization coming from the distribution of $T(Z)$. If this null hypothesis is rejected, either the energy functional or the stopping rule were not appropriate and should be chosen differently. This approach corresponds to the classical goodness-of-fit tests; here the observed data is the input $\mathcal{X}$ and the model is the particular algorithm (including the choice of the energy functional, the stopping rule, etc.) which produces the outputs.

If the test statistic T is scalar it is straightforward to assess how typical or extreme $T(\mathcal{X})$ is with respect to $T(\zeta_1), \ldots, T(\zeta_N)$, using empirical quantiles, see e.g. Loosmore and Ford (2006). If the test statistics T is functional it is possible to apply e.g. the extreme rank length version of the global envelope test (Mrkvička et al. 2018; Myllymäki et al. 2017), see also Narisetty and Nair (2016).

The choice of the test statistic is arbitrary and should be guided by the context of the practical problem at hand. If we used for testing the characteristics incorporated in the energy functional we would be essentially testing if the energy of the outputs is low enough, i.e. if the stopping rule is appropriate and/or the algorithm reaches acceptable local minima. While this is certainly of interest, non-rejection in such a test does not imply that other properties of the outputs match the properties of the input. Hence we believe it is beneficial to use other characteristics for testing than those used in the reconstruction procedure.

4.2 Testing in Simulation Studies

Assume now that the theoretical model for the point process X is known, as usual in simulation studies, and that a set of N outputs $\zeta_1, \ldots, \zeta_N$ based on possibly different input patterns (generated from X) has been produced. If it is possible to generate a large number of simulations $\mathcal{X}_1, \ldots, \mathcal{X}_K$ from the model, we compare for individual outputs ζ_k the value of the test statistics $T(\zeta_k)$ to the population $T(\mathcal{X}_1), \ldots, T(\mathcal{X}_K)$. Hence we, in fact, perform one test for each output. In this way, we are able to assess how well the properties of the outputs match those of the realisations from X. This is the key difference from the approach described in Section 4.1. Note that it is important to investigate a set of outputs based on different inputs in order to make the results less dependent on a particular realization of the input pattern.

In the simulation experiments presented in Section 5 we use the functional test statistics obtained by concatenating three morphological characteristics, area $A(r)$, boundary length $L(r)$ and Euler-Poincaré characteristic $\chi(r)$, described in Section 2.3, see also Mecke and Stoyan (2005)). The test statistics are their normalized versions: $T_1(r) = A(r)/n$, $T_2(r) = L(r)/n$, $T_3(r) = \chi(r)/n$ where n is the number of points of the point pattern in question. The normalization by the number of points is necessary in the simulation studies to achieve reasonable power of the test since the number of points in the simulated patterns $\mathcal{X}_1, \ldots, \mathcal{X}_K$ may vary greatly. We remark that this is not the case in Section 4.1 where the number of points in the input pattern and all the outputs is the same — in that case, the normalization by the number of points is not needed.

The three characteristics $T_1(r), T_2(r), T_3(r)$ are concatenated together and used to perform a single test on a specified significance level in order to avoid the multiple testing problem. In the following, we denote by $\mathcal{H}_m$ the null hypothesis that the distribution of the morphological characteristics of the output is the same as the distribution of the characteristics of the realizations generated by the model in question.

In the context of simulation studies, it is also possible to test whether the intensity function of the outputs matches the theoretical intensity function λ of the process X. We denote in the following the corresponding null hypothesis by $\mathcal{H}_\lambda$. We stress that such a test cannot be performed in practice where the theoretical intensity function is not known.

A test for detecting deviations from the assumed intensity function λ can be constructed as follows. Using the notation of Section 3.4, define the scalar test statistics T_λ as

$$T_\lambda(\zeta) = \sum_{i=1}^{I} a \left[\lambda(v_i) - \widehat{\lambda}_\zeta(v_i)\right]^2.$$

Comparing $T_\lambda(\zeta_k)$ to the population $T_\lambda(\mathcal{X}_1), \ldots, T_\lambda(\mathcal{X}_K)$ we obtain the result of the test for ζ_k (rejection/non-rejection). Finally, it is necessary to assess if the number of rejections is appropriate on a given significance level, using e.g. a confidence interval based on a binomial distribution.

We remark that even though the test statistic T_λ corresponds to the term Δ from Section 3.4, it is worth performing this test to assess if the required form of the intensity function is actually achieved, even with energy functionals containing Δ. It may be the case that the other terms in the energy functional outweigh Δ and the intensity function is not matched correctly.

5 Simulation Experiments

The aim of this section is to illustrate how the tests introduced in the previous section can be used to determine whether a given energy functional produces outputs that match the properties of the input. We perform a set of four experiments, each dealing with a different question. We focus on inputs generated from three different models (clustered, Poisson, regular) described in Section 5.2, all of them being inhomogeneous. Examples of outputs for the three models and several energy functionals are given in Online Resource 1, Figures S3 to S5.

In Experiment 1 we investigate if the approach from Wiegand et al. (2013) produces outputs that match the non-constant intensity function of the input (energy functionals E_3 and E_4, see Section 5.1). We compare the results with our approach from Section 3.4 where a term controlling the intensity function is included in the energy functional ($E_{3,\Delta}$ and $E_{3,\Gamma}$). Here we only perform the test of $\mathcal{H}_\lambda$ concerning the intensity function of the outputs.

Experiment 2 involves a larger set of energy functionals in order to examine if it is possible to reconstruct the inputs successfully, in terms of the morphological characteristics and the intensity function, using only a small number of summary characteristics (E_i and $E_{i,\Delta}$ for $i = 1, 2, 3, 5, 6, 7$). Here we perform both tests of $\mathcal{H}_m$ and $\mathcal{H}_\lambda$ to investigate both the topological properties of the outputs and their intensity function.

In Experiment 3 we focus on energy functionals consisting solely of empirical distribution functions (E_8, $E_{8,\Gamma}$ and E_9). In this case, the choice of weights is straightforward, as opposed to the general situation. Again we test both hypotheses $\mathcal{H}_m$ and $\mathcal{H}_\lambda$.

Finally, we present Experiment 4 in which we elaborate on Experiment 3 and investigate if the clustered model can be reconstructed more successfully if some prior knowledge of its structure is used when defining the energy functional (E_{10}, $E_{10,\Gamma}$ and E_{11}). This is motivated by not very convincing results for the clustered model in the previous experiments.

We stress here that the purpose of the simulation experiments is illustrative and we do not aim at identifying *a single best energy functional* if such a thing exists at all. The choice of the energy functional must always be related to the application at hand, including the choice of the summary characteristics f_j, weights w_{f_j} and ranges R_j.

5.1 Choice of Energy Functionals

Different energy functionals used in the simulation experiments are described in Table 1. Their choice is motivated by the conclusions of Wiegand et al. (2013) (roughly speaking, pair-correlation function g carries the most information about the patterns considered in the paper, but it should be combined with characteristics of a different distributional nature to provide more detailed description of the patterns) and by the different questions investigated in Experiments 1 to 4.

We consider the energy functional based solely on the inhomogeneous pair-correlation function g (E_1) and we also combine it with characteristics D_k based on interpoint distances (E_2, E_3). Furthermore, we combine g with F which describes, loosely speaking, gaps in the patterns and can carry some information about large-scale trends in the data (E_4), and also with the terms Δ, Γ proposed in this paper ($E_{1,\Delta}$, $E_{2,\Delta}$, $E_{3,\Delta}$, $E_{3,\Gamma}$).

We also investigate energy functionals obtained from the previous ones by replacing the inhomogeneous pair-correlation function g by the inhomogeneous L-function (E_i and $E_{i,\Delta}$ for $i = 5, \ldots, 7$). The motivation is that both of them carry the same information, only in a different form, and the non-parametric estimation of the L-function is much more

Table 1 Different energy functionals used in the simulation study

Energy functional	Summary characteristics	Weights	Experiments
E_1	g (inhomogeneous version)	1	2
$E_{1,\Delta}$	g, Δ	$10^2, 1$	2
E_2	g, D_1	1, 10	2
$E_{2,\Delta}$	g, D_1, Δ	$10^2, 10^3, 1$	2
E_3	$g, D_1, \ldots, D_{10}$	$1, 1, \ldots, 1$	1, 2
$E_{3,\Delta}$	$g, D_1, \ldots, D_{10}, \Delta$	$10^2, 10^2, \ldots, 10^2, 1$	1, 2
$E_{3,\Gamma}$	$g, D_1, \ldots, D_{10}, \Gamma$	$1, 12, \ldots, 1, 10$	1
E_4	$g, D_1, \ldots, D_{10}, F$	$1, 12, \ldots, 1, 1$	1
E_5	L (inhomogeneous version)	1	2
$E_{5,\Delta}$	L, Δ	$10^6, 1$	2
E_6	L, D_1	$10^3, 1$	2
$E_{6,\Delta}$	L, D_1, Δ	$10^6, 10^3, 1$	2
E_7	$L, D_1, \ldots, D_{10}$	$10^4, 1, \ldots, 1$	2
$E_{7,\Delta}$	$L, D_1, \ldots, D_{10}, \Delta$	$10^6, 10^2, \ldots, 10^2, 1$	2
E_8	$D_1, \ldots, D_{10}$	$1, \ldots, 1$	3
$E_{8,\Gamma}$	$D_1, \ldots, D_{10}, \Gamma$	$1, \ldots, 1, 10$	3
E_9	$D_1, \ldots, D_{10}, F$	$1, \ldots, 1, 1$	3
E_{10}	$D_1, \ldots, D_5$	$1, \ldots, 1$	4
$E_{10,\Gamma}$	$D_1, \ldots, D_5, \Gamma$	$1, \ldots, 1, 5$	4
E_{11}	$D_1, \ldots, D_5, F$	$1, \ldots, 1, 1$	4

straightforward as it does not require the choice of a smoothing kernel and its bandwidth. We use the L-function instead of the K-function since the variability of its estimate across different r values is stabilized by square root transformation.

Finally, we consider energy functionals based solely on empirical distribution functions (E_8, $E_{8,\Gamma}$, E_9, E_{10}, $E_{10,\Gamma}$, E_{11}). Here the choice of weights is straightforward since every characteristic included in the energy functional contributes with values on the same scale and it is easy to specify their relative importance.

While using the second-order characteristics g, L, the non-constant intensity function is taken into account. However, one should be aware that the L and g functions are derived in the context of SOIRS processes. We suggest using the empirical estimates of these characteristics even outside this context as they carry valuable information about interactions between pairs of points. In such a situation we treat them as empirical descriptors only, without relation to any theoretical characteristic. Similarly, we use the empirical distribution functions $\widehat{D}_k$, $\widehat{F}$ even outside the context of stationary processes, merely as empirical descriptors rather than estimators of a theoretical characteristic, as they carry important information about the geometry of the patterns in question.

Also, we use the estimators (2), (3) without any edge-correction to reduce the computational load. This means that the values of $\widehat{D}_k$, $\widehat{F}$ are affected by the size and shape of the observation window W. However, this is acceptable in this simulation study since all the configurations, input, intermediate and output, are confined to the same window W.

The weights are given in the third column of Table 1 and were chosen based on prior experiments so that each term contributes to the total energy by values on the same scale. We use the same weights for all the three models considered below, which necessarily required some compromise. If only a single model was considered the weights could be chosen more specifically, resulting presumably in more successful reconstructions. The last column of Table 1 provides an indication in which experiments the given energy functional was used.

5.2 Theoretical Models

The theoretical models for X considered in this study are a thinned Thomas process, an inhomogeneous Poisson process and a geometrically transformed Matérn hard-core process of type II, respectively (Daley and Vere-Jones 2008; Illian et al. 2004; Møller and Waagepetersen 2004). Parameters of these models are chosen so that the three models have the same intensity function. The observation window is $W = [0, 1]^2$ in all cases.

The Thomas process is a typical example of clustered processes which are of particular interest in ecological applications where the stochastic reconstruction approach has become popular. The Poisson point process often serves as a benchmark model to which other processes are compared. To cover also the case of regular processes we include the Matérn hard-core process of type II. Figure 2 shows realizations simulated from the three models.

We first consider a stationary (modified) Thomas process in $\mathbb{R}^2$ with the intensity of parents $\kappa = 40$, the mean number of offspring per parent $\mu = 6$ and the standard deviation of the bivariate Gaussian distribution governing the placement of offspring relative to the parents $\sigma = 0.015$. The inhomogeneous Thomas process is then constructed by applying location-dependent thinning using the thinning function $f(x)$ specified below. Such a process has the SOIRS property, see Baddeley (2000, p.331), and its intensity function is given by

$$\lambda(x) = 240 f(x), \quad x \in \mathbb{R}^2. \tag{5}$$

Furthermore, we consider the inhomogeneous Poisson point process in $\mathbb{R}^2$ with the intensity function (5). This process also has the SOIRS property.

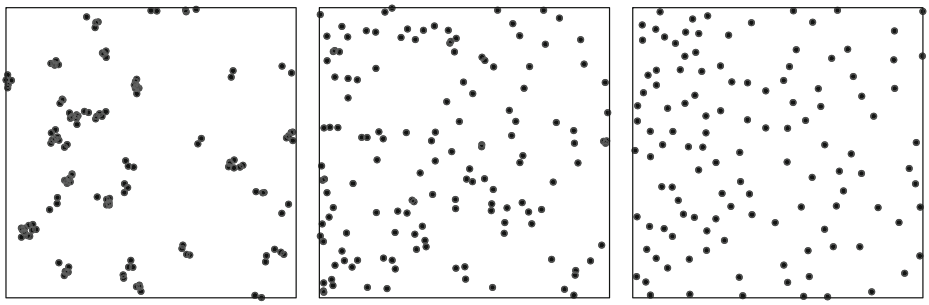

Fig. 2 From left to right: realisation of the thinned Thomas process, the inhomogeneous Poisson process and the transformed Matérn hard-core process of type II. For details see the main text

Finally, we consider the stationary Matérn hard-core process of type II in $\mathbb{R}^2$ with the intensity of the underlying Poisson point process $\kappa = 300$ and the hard-core distance $r = 0.05$. The intensity of the stationary hard-core process is

$$\tau = \left(1 - e^{-\kappa\pi r^2}\right) / \left(\pi r^2\right).$$

Then to each point we apply the exponential transformation

$$c(x) = \frac{1}{e^b - 1}\left(e^{b x_1} - 1\right), \quad x = (x_1, x_2) \in \mathbb{R}^2,$$

where $b = 1.3$, and restrict the process to the unit square W. The intensity function of the transformed process on W is

$$\tau(e^b - 1)e^{-b x_1}/b.$$

Note that the hard-core distance in the transformed process changes along the x_1-axis. This process does not have the SOIRS property.

To obtain the same intensity function also for the clustered and Poisson models we need to use in (5) the following function $f(x)$:

$$f(x) = \min\left\{K e^{-b x_1}, 1\right\}, \quad x = (x_1, x_2) \in \mathbb{R}^2, \quad K = \frac{\tau(e^b - 1)}{240b}.$$

Note that each of the three models considered here has specific properties, important in the following experiments. The realizations of the clustered model have clusters of points placed randomly in the observation window, resulting in a high variation of the estimated intensity functions. When reconstructing inputs generated from the Poisson model, the starting configuration—realization of the binomial point process with appropriate non-constant intensity function—already has all the required properties and running the algorithm may only violate them. In the transformed Matérn process the changing hard-core distance makes it difficult to describe the interpoint interactions using summary characteristics designed for stationary or SOIRS processes.

5.3 Design of the Simulation Study

For each of the three models described above, we simulate 50 independent realisations in the observation window $W = [0, 1]^2$. These are used as inputs of the stochastic reconstruction algorithm. For each input and each energy functional we perform 20 independent runs of

the stochastic reconstruction algorithm, obtaining 20 outputs. Multiple inputs are used to capture the variability of the models, whereas multiple outputs deal with the variability introduced by the algorithm itself.

In this manner, 1000 outputs are obtained for each model and each energy functional considered in the individual experiments. For each output, we perform the two Monte Carlo tests described in Section 4, if applicable in the given experiment. That is we simulate a large number of independent realisations from the model and assess how typical or extreme the given output is w.r.t. the population of simulated realisations. The test of $\mathcal{H}_m$ is based on 999 simulations from the null model (in order to reduce the computational load), the test of $\mathcal{H}_\lambda$ is based on 2499 simulations. Both tests are performed on the significance level $\alpha = 0.05$ and hence we expect approx. 50 outputs out of 1000 to result in rejection. In fact, the 95% confidence interval for the number of rejections is (37,64). Therefore, we expect to see between 3.7% and 6.4% of rejected outputs.

5.4 Software Implementation and Choice of Tuning Parameters

The source codes for the stochastic reconstruction algorithm discussed in this paper are available upon request. This simulation experiments are performed in `R` (version 3.4.3) with standard packages `spatstat` (version 1.55-0) and `TDA` (version 1.6) and package `GET` (version 0.1, Myllymäki et al. 2018).

The intensity function of all realisations is estimated using the function `density.ppp` from the `spatstat` package, with default settings. The pair-correlation function is estimated using the `pcfinhom` from the same package, with default settings except from the slight modification of the denominator described in Baddeley et al. (2015, p.229). Translation edge-correction is used for estimation of the pair-correlation function and the L-function.

The constants R_j are set to be 0.2 for the pair-correlation function and the L-function. After plotting $\widehat{F}$ and $\widehat{D}_k(r)$ for several realisations from the given models we set $R_j = 0.3$ for F and D_k, $k = 1, 2, \ldots, 10$, to cover almost the whole range of values of the empirical distribution functions.

The stopping rule is chosen so that the run of the algorithm stops if proposed configurations are not accepted for 100 times in a row.

The morphological characteristics $A(r)$, $L(r)$ and $\chi(r)$ used for testing $\mathcal{H}_m$ are computed using functions `dilated.areas, discs, perimeter` from the `spatstat` package and the function `alphaComplexDiag` from the `TDA` package. The range of argument r is for all three characteristics [0,0.2] for the clustered model and [0,0.15] for the Poisson and regular model.

5.5 Results

The tables below report the percentage of rejected reconstructions for the considered energy functionals in tests of $\mathcal{H}_m$ and $\mathcal{H}_\lambda$. The input realisations are tested in the same way as the outputs to determine how typical or extreme the realisation is w.r.t. the population of simulated realisations.[1] This is useful for a detailed inspection of the results since it often happens that a single input, which is considered extreme w.r.t. the population of simulations

[1]Detailed tables containing the p-values of input realisations as well as the exact number of rejected reconstructions for individual tests, models and energy functionals are available at http://msekce.karlin.mff.cuni.cz/~dvorak/supplementary/StochasticReconstruction.html

(it has p-value ≤ 0.05 itself), produces most of the outputs causing rejections for a given model and energy functional. Also, only 1 input out of 50 in our study produced p-value ≤ 0.05 in the test of $\mathcal{H}_\lambda$ for the Poisson model and also for the hard-core model. This results, for some energy functionals, in the percentage of rejections of $\mathcal{H}_\lambda$ being considerably smaller than 5 %, without indicating any issue.

Experiment 1

In this experiment we examine the approach of Wiegand et al. (2013) using the energy functionals based on combination of g, D_k and F (E_3, E_4). We investigate, using the test of $\mathcal{H}_\lambda$, whether the intensity function of the outputs matches the intensity function of the inputs. Table 2 indicates that the reconstructions are not adequate in terms of intensity function, the percentage of rejections ranging from 20 % to 60 % for tests on the nominal 5 % level.

When considering energy functional E_3 but incorporating a term controlling the intensity function ($E_{3,\Delta}$, $E_{3,\Gamma}$) the reconstructions are more successful, see Table 2, and in fact acceptable for $E_{3,\Delta}$. We observe that using the term Γ is relevant for the clustered process which confirms our expectation, see Section 3.4. On the other hand, for the Poisson and hard-core models the variability of the intensity function estimated from simulated realizations is much smaller than for the clustered process and hence a term more strictly controlling the intensity function, such as Δ, is required.

Experiment 2

In the second experiment we investigate a variety of different energy functionals combining g or L with D_k (E_1 to E_3 and E_5 to E_7) and possibly with Δ ($E_{1,\Delta}$ to $E_{3,\Delta}$ and $E_{5,\Delta}$ to $E_{7,\Delta}$). The question of interest is whether using a combination of a small number of summary characteristics can produce appropriate reconstructions in terms of both $\mathcal{H}_m$ and $\mathcal{H}_\lambda$ (using high number of characteristics makes the choice of weights more complicated and increases the risk of overfitting—reducing the variability of the outputs below the variability of realizations from the assumed model).

Table 3 indicates that only energy functionals incorporating the term Δ were successful in matching the intensity function of the inputs. Only for these energy functionals the percentage of rejections in the test of $\mathcal{H}_\lambda$ is close to 5 %. Hence in the following discussion we restrict our attention to the functionals $E_{i,\Delta}$, $i = 1, 2, 3, 5, 6, 7$.

Generally speaking, including more summary characteristics in the energy functional results in fewer rejections of $\mathcal{H}_m$ for all three models considered here, see Table 3.

For the Poisson model, all energy functionals containing Δ perform similarly and provide satisfactory outputs. We observe that the properties of the starting configuration are not violated by the algorithm.

Table 2 Experiment 1: percentage of rejections in the test of the hypothesis $\mathcal{H}_\lambda$ on the nominal 5 % level for selected energy functionals

Energy functional		Thomas	Poisson	Matérn
E_3	$g, D_1, \ldots, D_{10}$	29.4	22.4	58.3
E_4	$g, D_1, \ldots, D_{10}, F$	28.6	24.2	55.9
$E_{3,\Delta}$	$g, D_1, \ldots, D_{10}, \Delta$	6.9	3.0	2.9
$E_{3,\Gamma}$	$g, D_1, \ldots, D_{10}, \Gamma$	9.0	17.7	30.0

Table 3 Experiment 2: percentage of rejections in the test of the hypotheses $\mathcal{H}_m$ and $\mathcal{H}_\lambda$ on the nominal 5 % level for selected energy functionals

Energy functional		Thomas		Poisson		Matérn	
		$\mathcal{H}_m$	$\mathcal{H}_\lambda$	$\mathcal{H}_m$	$\mathcal{H}_\lambda$	$\mathcal{H}_m$	$\mathcal{H}_\lambda$
E_1	g	54.3	25.7	10.3	28.4	40.7	55.6
$E_{1,\Delta}$	g, Δ	33.2	6.5	8.3	3.0	79.9	2.6
E_2	g, D_1	16.6	24.5	6.3	25.7	15.4	65.7
$E_{2,\Delta}$	g, D_1, Δ	13.3	6.6	5.9	3.1	28.5	2.9
E_3	$g, D_1, \ldots, D_{10}$	13.3	29.4	5.5	22.4	58.3	58.3
$E_{3,\Delta}$	$g, D_1, \ldots, D_{10}, \Delta$	11.4	6.9	6.7	3.0	73.8	2.9
E_5	L	44.1	10.6	9.0	24.5	6.9	57.1
$E_{5,\Delta}$	L, Δ	35.3	6.0	7.3	2.8	8.0	3.0
E_6	L, D_1	12.3	11.6	6.8	27.2	6.5	52.9
$E_{6,\Delta}$	L, D_1, Δ	13.3	5.8	5.4	3.3	5.9	5.0
E_7	$L, D_1, \ldots, D_{10}$	10.3	15.2	5.6	24.7	7.2	48.3
$E_{7,\Delta}$	$L, D_1, \ldots, D_{10}, \Delta$	12.4	5.8	7.4	2.8	5.6	5.5

For the hard-core model using the L-function instead of the pair-correlation function g turns out to be more successful. The reason is that a kernel estimate of g somewhat blurs the hard-core distance and in the outputs, we can often observe pairs of points too close together. This does not happen with the L-function.

For the clustered model the outputs are not quite satisfactory, the percentage of rejections of $\mathcal{H}_m$ being at least twice as high as the nominal level of the test. This is related to the fact that, together with g or L, using only D_1 does not bring enough information about the structure of the individual clusters, the mean number of points in a cluster being 6. On the other hand, using D_1 to D_{10} means we try to reconstruct not only the geometry of the clusters but also their mutual positions. This motivated Experiment 4 where some prior information on the typical cluster size is assumed. Furthermore, using different weights could also improve the performance of the reconstruction procedure.

Experiment 3

The next experiment is motivated by the difficulties in choosing weights giving relative importance of the individual terms in the energy functional. Here we abandon g, L and Δ and focus on energy functionals consisting solely of empirical distribution functions. Hence the range of values is the same for all individual terms and it is straightforward to choose the weights, directly specifying the relative importance.

Table 4 summarizes the results of Experiment 3. Clearly, the chosen energy functionals are not successful in matching the intensity function, i.e. the percentage of rejections in the test of $\mathcal{H}_\lambda$ is too high for all three models. For the Poisson model, the morphological properties of the patterns are matched correctly with all three energy functionals. The opposite holds for the hard-core model. This is caused by the $\widehat{D}_k$ not carrying any information about how the interpoint distances are distributed in W, as opposed to g and L which incorporate the information about the intensity function.

Table 4 Experiment 3: percentage of rejections in the test of the hypotheses $\mathcal{H}_m$ and $\mathcal{H}_\lambda$ on the nominal 5 % level for selected energy functionals consisting only of empirical distribution functions

Energy functional		Thomas		Poisson		Matérn	
		$\mathcal{H}_m$	$\mathcal{H}_\lambda$	$\mathcal{H}_m$	$\mathcal{H}_\lambda$	$\mathcal{H}_m$	$\mathcal{H}_\lambda$
E_8	$D_1, \ldots, D_{10}$	13.5	30.9	5.1	22.6	75.8	65.5
E_9	$D_1, \ldots, D_{10}, F$	7.4	28.9	3.9	21.1	78.5	64.4
$E_{8,\Gamma}$	$D_1, \ldots, D_{10}, \Gamma$	12.3	8.1	3.2	18.7	95.2	30.7

For the clustered model the functional $E_{8,\Gamma}$ performs best but is not completely successful in matching the morphological properties. This is again linked to the fact that using empirical distribution functions of distances up to 10th neighbour acknowledges not only the structure of individual clusters but also their mutual arrangement. This is not desirable and we elaborate on this issue in the following experiment.

Experiment 4

The last experiment focuses only on the clustered model and assumes that some prior information on the typical number of points in a cluster is known. We aim at using energy functionals with D_k for k close to the mean number of points in a cluster. For the cluster model considered here, this equals 6 and we use D_1 up to D_5 in the energy functionals. We again restrict our attention to empirical distribution functions only to make the choice of weights simple.

Table 5 shows that it is possible to achieve satisfactory reconstructions using this approach but a term directly controlling the intensity function needs to be incorporated in the energy functional ($E_{10,\Gamma}$).

6 Discussion

In the present paper, we have discussed the possibility of using the stochastic reconstruction algorithm for inhomogeneous point patterns. We have established a general framework for formally testing the quality of outputs of the algorithm, using two tests based on morphological characteristics A, L, χ, focusing on the geometric properties of the point patterns, and on the estimated intensity function. The two tests deal with complementary properties of the point patterns and we believe that it is beneficial to perform both tests.

Table 5 Experiment 4, clustered model: percentage of rejections in the test of the hypotheses $\mathcal{H}_m$ and $\mathcal{H}_\lambda$ on the nominal 5 % level for selected energy functionals consisting only of empirical distribution functions, using prior knowledge about the mean number of points in a cluster

Energy functional		$\mathcal{H}_m$	$\mathcal{H}_\lambda$
E_{10}	$D_1, \ldots, D_5$	14.1	50.8
E_{11}	$D_1, \ldots, D_5, F$	4.0	40.2
$E_{10,\Gamma}$	$D_1, \ldots, D_5, \Gamma$	6.4	7.1

We have illustrated in simulation experiments, using the test of the hypothesis $\mathcal{H}_\lambda$ proposed here, that the version of the algorithm available in the literature for inhomogeneous point patterns does not produce acceptable outputs – the non-constant intensity function is not matched correctly.

We have proposed adding an extra term Δ to the energy functional in order to control directly the intensity function of the outputs. This remedies the issue with the intensity function for all of the considered models, clustered, Poisson and regular. For reconstruction of clustered patterns, it may be appropriate in a given application to use the term Γ in the energy functional instead, which controls only the values of the estimated intensity function, not their arrangement in the observation window. In this way, the cluster geometry is reconstructed but the clusters may appear in different locations in the outputs than in the input.

We have demonstrated that all the three models considered here can be successfully reconstructed using a small set of summary characteristics, provided that the intensity function is controlled directly in the energy functional and that specific features of the input pattern are taken into account. For the clustered model, prior information on the cluster size was needed. For the Poisson model, it was enough to control the intensity function and the way of controlling the interactions was not crucial. For the regular model, it was beneficial to use the L-function instead of the pair-correlation function to better account for the hard-core property of the input pattern. All of this considered, our findings support the claim made in Wiegand et al. (2013) that more than one type of summary characteristic should be incorporated in the energy functional in order to obtain satisfactory outputs.

References

Baddeley A, Møller J, Waagepetersen RP (2000) Non-and semiparametric estimation of interaction in inhomogeneous point patterns. Stat Neerl 54:329–350

Baddeley A, Rubak E, Turner R (2015) Spatial Point patterns: Methodology and Applications with R. Chapman & hall/CRC, Boca Raton

Daley D, Vere-Jones D (2008) An Introduction to the Theory of Point Processes. Volume II: General Theory and Structure, 2nd edn. Springer, New York

Getzin S, Wiegand T, Hubbell SP (2014) Stochastically driven adult-recruit associations of tree species on Barro Colorado Island. Proc R Soc B 281:20140922

Illian J, Penttinen A, Stoyan H, Stoyan D (2004) Statistical Analysis and Modelling of Spatial Point Patterns. Wiley, Chichester

Jacquemyn H, Brys R, Honnay O, Roldán-Ruiz I, Lievens B, Wiegand T (2012) Nonrandom spatial structuring of orchids in a hybrid zone of three Orchis species. New Phytol 193:454–464

Koňasová K (2018) Stochastic reconstruction of random point patterns, Master thesis, Charles University, Czech Republic. Available online: http://hdl.handle.net/20.500.11956/98703 [cited 13. 12. 2018]

Lilleleht A, Sims A, Pommerening A (2014) Spatial forest structure reconstruction as a strategy for mitigating edge-bias in circular monitoring plots. For Ecol Manag 316:47–53

Loosmore BN, Ford DE (2006) Statistical inference using the g or K point pattern spatial statistics. Ecology 87:1925–1931

Mecke KR, Stoyan D (2005) Morphological characterization of point patterns. Biom J 47:473–488

Møller J, Waagepetersen RP (2004) Statistical Inference and Simulation for Spatial Point Processes. Chapman & Hall/CRC, Boca Raton

Mrkvička T, Hahn U, Myllymäki M (2018) A one-way ANOVA test for functional data with graphical interpretation. Available on arXiv:1612.03608 [cited 26. 11. 2018]

Mundo I, Wiegand T, Kanagaraj R, Kitzberger T (2013) Environmental drivers and spatial dependency in wildfire ignition patterns of northwestern Patagonia. J Environ Manag 123:77–87

Myllymäki M, Mrkvička T, Grabarnik P, Seijo H, Hahn U (2017) Global envelope tests for spatial processes. J R Stat Soc Ser B 79:381–404

Myllymäki M, Mrkvička T, Grabarnik P, Seijo H, Hahn U (2018) Global Envelope Tests. R package version 0.1. https://github.com/myllym/GET [cited 17. 12. 2018]
Narisetty NN, Nair VJ (2016) Extremal depth for functional data and applications. J Am Stat Assoc 111:1705–1714
Pommerening A (2006) Evaluating structural indices by reversing forest structural analysis. For Ecol Manag 224:266–277
Stoyan D, Stoyan H (1994) Fractals, Random Shapes and Point Fields. Wiley, Chichester
Torquato S (2002) Random Heterogeneous Materials. Microstructure and Macroscopic Properties. Springer, New York
Tscheschel A, Stoyan D (2006) Statistical reconstruction of random point patterns. Comput Stat Data Anal 51:859–871
Tscheschel A, Chiu SN (2008) Quasi-plus sampling edge correction for spatial point patterns. Comput Stat Data Anal 52:5287–5295
Wiegand T, He F, Hubbell SP (2013) A systematic comparison of summary characteristics for quantifying point patterns in ecology. Ecography 36:92–103
Wong KY, Chiu SN (2016) Isotropy test for spatial point processes using stochastic reconstruction. Spat Stat-Neth 15:56–69

Publisher's Note Springer Nature remains neutral with regard to jurisdictional claims in published maps and institutional affiliations.